Chapman University

Chapman University Digital Commons

Institute for ECHO Articles and Research

Institute for Earth, Computing, Human and Observing (ECHO)

10-17-2020

Assessment of Aerosol Optical Depth Under Background and Polluted Conditions Using AERONET and VIIRS Datasets

Mijin Kim
NASA-Goddard Space Flight Center

Seung Hee Kim
Chapman University, sekim@chapman.edu

Woogyung Vincent Kim
NASA-Goddard Space Flight Center

Yun Gon Lee
Chungnam National University

Jhoon Kim
Yonsei University

See next page for additional authors

Follow this and additional works at: https://digitalcommons.chapman.edu/echo_articles

 Part of the Atmospheric Sciences Commons, Environmental Indicators and Impact Assessment Commons, Environmental Monitoring Commons, and the Other Oceanography and Atmospheric Sciences and Meteorology Commons

Recommended Citation

Kim, M., Kim, S.H., Kim, W.V., Lee, Y.G., Kim, J., Kafatos, M.C., 2021. Assessment of aerosol optical depth under background and polluted conditions using AERONET and VIIRS datasets. Atmospheric Environment 245, 117994. https://doi.org/10.1016/j.atmosenv.2020.117994

This Article is brought to you for free and open access by the Institute for Earth, Computing, Human and Observing (ECHO) at Chapman University Digital Commons. It has been accepted for inclusion in Institute for ECHO Articles and Research by an authorized administrator of Chapman University Digital Commons. For more information, please contact laughtin@chapman.edu.

Assessment of Aerosol Optical Depth Under Background and Polluted Conditions Using AERONET and VIIRS Datasets

Comments

NOTICE: this is the author's version of a work that was accepted for publication in *Atmospheric Environment*. Changes resulting from the publishing process, such as peer review, editing, corrections, structural formatting, and other quality control mechanisms may not be reflected in this document. Changes may have been made to this work since it was submitted for publication. A definitive version was subsequently published in *Atmospheric Environment*, volume 245, in 2021. https://doi.org/10.1016/j.atmosenv.2020.117994

The Creative Commons license below applies only to this version of the article.

Creative Commons License

This work is licensed under a Creative Commons Attribution-Noncommercial-No Derivative Works 4.0 License.

Copyright

Elsevier

Authors

Mijin Kim, Seung Hee Kim, Woogyung Vincent Kim, Yun Gon Lee, Jhoon Kim, and Menas C. Kafatos

This article is available at Chapman University Digital Commons: https://digitalcommons.chapman.edu/echo_articles/3

Assessment of Aerosol Optical Depth Under Background and Polluted Conditions Using AERONET and VIIRS Datasets

Mijin Kim[1,2], Seung Hee Kim[3]*, Woogyung Vincent Kim[1,4], Yun Gon Lee[5], Jhoon Kim[6], and Menas C. Kafatos[3]

[1]NASA-Goddard Space Flight Center (GSFC), Greenbelt, MD 20771-0001, USA

[2]Universities Space Research Association (USRA), Columbia, MD 21046, USA

[3]The Center of Excellence in Earth Systems Modeling & Observations (CEESMO), Chapman University, Orange, CA 92866, USA

[4]Earth System Science Interdisciplinary Center (ESSIC), University of Maryland, College Park, MD 20737, USA

[5]Department of Atmospheric Sciences, Chungnam National University, Daejeon, Republic of Korea

[6]Department of Atmospheric Sciences, Yonsei University, Seoul, Republic of Korea

Abstract

We investigated aerosol optical depth (AOD) under background and polluted conditions using Aerosol Robotic Network (AERONET) and Visible Infrared Imaging Radiometer Suite (VIIRS) observations. The AOD data were separated into background, high, and median AOD (BAOD, HAOD, and MAOD, respectively) based on the cumulative AOD distribution at each point and then their spatiotemporal variations were analyzed. Persistent pollutant emissions from industrial activity in South Asia (SUA) and Northeast Asia (NEA) produced the highest BAOD values. Gridded-BAODs obtained from VIIRS Deep Blue AOD products showed widespread high-level BAOD over the oceans associated with transport from dust and biomass burning events. The temporal variations in BAOD and HAOD were generally consistent with that of MAOD, but differences were found in seasonal variation as well as in long-term trends in some regions. Southeast Asia (SEA) and South America/South Africa (SAM/SAF) showed similar HAOD levels owing to biomass burning, but BAODs were higher in SEA than in SAM/SAF. In NEA, BAOD was lowest during the summer rainy season, as opposed to the peaks in MAOD and HAOD. Long-term trends of the AODs show clear regional characteristics. The AODs have decreasing trends in NEA, Europe/Mediterranean basin, and Northeast America but increasing trends in SUA, and in North Africa and the Middle East. The trend of HAOD in Northwest America and Australia was opposite to that of BAOD. The spatiotemporal patterns of the HAOD and BAOD provide detailed information on changes in aerosol loading compared to using only MAOD.

Keywords: Background aerosol optical depth, AERONET, VIIRS Deep blue aerosol, linear AOD trend

1. Introduction

Aerosols play an important role in the Earth's energy budget as they interact with solar and infrared radiation and modify cloud microphysics (IPCC, 2013). Aerosols contribute to a cooling of the Earth's surface temperature (Kaufman et al., 2002), and their complicated chemical and physical properties lead to large uncertainties in projection of climate change. Various Earth-observing platforms have measured aerosol amounts and trends to quantify the impact of aerosol radiative forcing on climate change. Ground- and satellite-based remote sensing techniques have provided long-term data for aerosol optical depth (AOD) over the entire globe and have contributed to a better understanding of the spatiotemporal variability of aerosols.

Producing accurate and reliable AOD data is a crucial step in assessing the impacts of aerosol on the climate and there have been numerous efforts to improve the quality of the datasets. In an AOD retrieval algorithm, separating surface and atmospheric contributions to the measured top-of-atmosphere (TOA) reflectance is essential. However, complex land surface properties make surface reflectance estimation a challenging issue. Recent studies have shown that when the algorithm relies on atmospherically corrected surface reflectance, considering background aerosol optical depth (BAOD) reduces the uncertainty in satellite-based AOD remote sensing (Kim et al., 2014, 2016, Knapp et al., 2005, Zhang et al., 2011, Zhang et al., 2016). For example, a single visible channel algorithm utilizing minimum reflectance method (Kim et al., 2016) showed a 7% overestimation in surface reflectance of 0.05, and ignored a BAOD of 0.05. The overestimation in surface reflectance led to an 11% underestimation in AOD of 0.45 (at 550 nm).

Existence of the BAOD has recognized with non-zero aerosol loading under minimal anthropogenic activities. Previous studies have defined the BAOD as

minimum AOD value by measuring remote region (Halthore et al., 1998; Halthore and Caffrey, 2006; Holben et al., 2001). Other study described it as an AOD value during the small temporal variation (Kaufman et al., 2001). Thereafter, studies have defined the BAOD in various ways from a perspective of satellite-based aerosol remote sensing and have reported spatiotemporal variation. The Geostationary Operational Environmental Satellite (GOES) Aerosol/Smoke Product (GASP) algorithm adopted a constant BAOD of 0.02 and showed enhancement in surface reflectance estimation (Zhang et al., 2011). Kim et al. (2014) defined BAOD as the second minimum value of Aerosol Robotic Network (AERONET) direct measurements (Holben et al., 1998; http://aeronet.gsfc.nasa.gov/) in each month, and applied the monthly BAOD to AOD retrieval in the Hong Kong area. Kim et al. (2016) employed the gridded-BAOD, which was obtained from the Moderate Resolution Imaging Spectroradiometer (MODIS) level 2 aerosol product in the AOD retrieval algorithm over Northeast Asia. Zhang et al. (2016) estimated BAOD as the lowest 5^{th} percentile of AOD measured at each AERONET site and interpolated the value at each $0.1° \times 0.1°$ grid box using inverse distance weighting. BAOD can vary widely depending on natural emission phenomena and meteorological conditions. The studies investigating spatial BAOD distribution represented that anthropogenic activity (e.g., industrialization, population growth, and land-use change) results in the accumulation of pollutants in the atmosphere and consequently induces high BAOD near the source regions.

Though previous studies established for the importance of BAOD, there is still a lack of comprehensive analyses of temporal and spatial variations in BAOD. Land use change, anthropogenic activity, and meteorological conditions are known to cause seasonal variations in aerosol loading, but current understanding of BAOD variations is limited. Understanding the spatiotemporal variation in BAOD is not only essential

for improving remote sensing products but is also helpful for monitoring air quality in relation to the accumulation of pollutants in source regions. Long-term variation in BAOD depends on changes in meteorological conditions, economic growth, and restrictions on pollutant emissions (Yoon et al., 2016).

Ground-based AERONET stations are sparsely deployed over the ocean and remote regions that are affected by both long-range transport from continents and natural aerosol emission such as VOCs and sea salts. The sparse placement of AERONET sun-photometers over remote regions limits the ability of the network to measure BAOD with minimal anthropogenic effects. In this regard, we analyzed spatial and seasonal BAOD variations based on both AERONET direct measurements that have high accuracy but limited coverage, and VIIRS Deep Blue (DB) level 2 aerosol products that cover the entire globe and can therefore fill spatial gaps in the AERONET data (Hsu et al., 2019, Sayer et al., 2018a). We define BAOD as the average of the lowest 5% of AODs from a cumulative AOD distribution, as suggested by Zhang et al. (2016) and Yoon et al. (2016). High-AOD (HAOD) was also identified as the highest 5%, and compared with BAOD and median AOD (MAOD).

The remainder of the manuscript is organized as follows. Details of the datasets and methodology for AOD analysis are described in Section 2, and the analysis of AERONET- and VIIRS-based BAOD and HAOD are discussed in Section 3. In Section 3.1, the global distributions of BAOD and HAOD are presented, and their temporal changes are shown in terms of seasonal variation. Global BAODs and HAODs obtained from VIIRS DB aerosol products are presented in Section 3.2. Long-term trends of the seasonal AODs that we obtained are discussed in Section 3.3. Section 4 summarizes and discusses our results, and conclusions are provided in Section 5.

2. Data and Methods

2.1. AOD from AERONET sun-photometers

AERONET has recorded >25 years of aerosol properties, and the number of sites has increased to >600 as of 2018 (Giles et al., 2019). The dataset from AERONET contains valuable information for understanding global aerosol properties even though the stations are not equally distributed in remote regions. An advantage of this ground-based dataset is its higher accuracy in AOD measurements than other datasets. The uncertainty of a newly calibrated field instrument under cloud-free conditions is lower than ±0.01 for wavelengths longer than 440 nm (Eck et al., 1999, Giles et al., 2019). Recently, the AERONET algorithm has been updated to Version 3 with significant improvement in cloud screening and instrument anomaly quality control (Giles et al., 2019).

The AERONET AOD dataset is widely used as ground truth because it has a well-defined low level of uncertainty. This study employs the quality-assured Level 2.0 daily-AOD provided by the AERONET Version 3 algorithm. In addition, daily averaged AOD products with a long time series were adopted to minimize the possible bias in low and high AOD measurements induced by instrument calibration error and cloud contamination, respectively.

At each AERONET site, BAOD and HAOD are calculated by averaging the AODs below the lowest 5^{th} and above the highest 5^{th} percentile of a cumulative AOD distribution, respectively (Zhang et al., 2016, Yoon et al., 2016). An AERONET site is selected for analysis when there are valid AODs for >750 days over a period of 5 years or more. For seasonal analyses, AOD measurements of at least 90 days are compiled per season during the total data period to calculate seasonal BAODs and HAODs. To

assess long-term changes, BAODs and HAODs are calculated per season. Details of the trend analysis are given in Section 2.4.

2.2. AOD from the VIIRS Deep Blue and SOAR algorithms

The DB aerosol products from VIIRS cover all cloud-free and snow-free surfaces over land and ocean with ~6 km resolution (at nadir). The algorithm consists of two main algorithms: the DB (Hsu et al., 2019) for land and the Satellite Ocean Aerosol Retrieval (SOAR; Sayer et al. 2018a) for ocean. The SOAR algorithm has two processing paths for the full and backup algorithms, which cover 95% of water pixels and the remaining 5% shallow or turbid pixels, respectively. In a comparison with AERONET AOD for land products, 80% of matchups agreed within the expected error range of ±(0.05 + 20%) (Hsu et al. 2019); for ocean products, 66% of matchups fell within the expected error range of ±(0.03 + 10%) for the full and ±(0.03 + 15%) for the backup algorithm (Sayer et al., 2018b). The correlation coefficient and the median bias between VIIRS DB AODs and AERONET AODs are 0.82 and 0.005, respectively. Spatial patterns of the comparison show that the correlation coefficients are close to 1 and the bias is generally ±0.02 over the Americas and Eurasia. The bias tends to be more negative in some biomass burning regions (Hsu et al., 2019). The AOD group lower than 0.2 has a positive bias of about 0.02 related to the calibration uncertainties and the surface reflectance model (Sayer et al., 2019).

VIIRS Deep Blue Level 2 aerosol products are used in this study to fill the gaps in the BAOD estimation over oceans and remote regions where AERONET instruments are not available. We averaged the Level 2 AOD into a 0.25° × 0.25° grid to obtain daily AOD maps from March 2012 to February 2019.

2.3. BAOD and HAOD in the AOD distribution

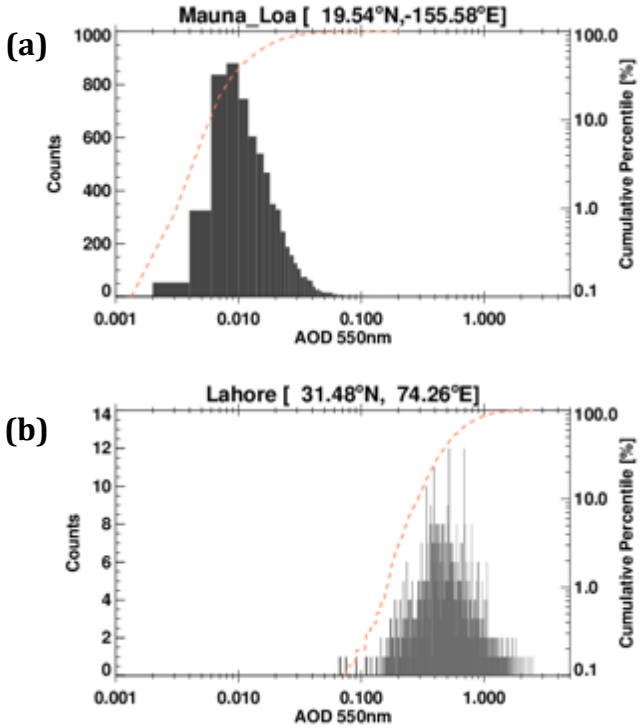

Figure 1. Histogram of aerosol optical depth (AOD) at 550 nm obtained from sun-photometer measurement at (a) Mauna Loa from 1994 to 2019 and (b) Lahore from 2006 to 2015. The dashed orange line shows the cumulative percentile.

Analyzing the MAOD from the uni-modal density distribution is a common approach to investigating the central tendency of temporal variations in AOD. In the present study, however, we employ low and high percentiles to present variations in AOD over asymmetric distributions. The low-percentile AOD, defined as BAOD, reflects persistent aerosol loads rather than episodic events. For example, the AODs at Mauna Loa [19.54°N, –155.58°E], where there are minimal anthropogenic emissions and occasional aerosol inflows, retain a narrow range of variation with low-level BAOD in the right-skewed density distribution (Figure 1a). In contrast, persistent pollutant inflows from anthropogenic activity and dust transport from the Arabian Desert at Lahore, Pakistan [31.48°N, 74.26°E], shift the AOD density distribution and increase the BAOD due to particles accumulating in the atmosphere (Figure 1(b)).

The upper boundary of AOD, the HAOD, is related to severe aerosol events, whereas BAOD is affected by continuous aerosol emissions. Since HAOD can increase as a result of a few extreme aerosol events, remarkable spatial variation is unlikely. Its temporal variation in a given location, however, can indicate a heavy aerosol-emission event. HAOD can be biased by cloud contamination, even when using high-quality AOD measurement instruments. Therefore, we analyze the relative differences in HAOD variability assuming that biases occur randomly and thus do not change the tendency of spatial variation or long-term HAOD trends.

2.4. Calculation of a long-term trend

Because BAOD represents the accumulation of aerosol, long-term BAOD trends can be an indicator of changes in air quality. For example, efforts to reduce air pollutant emissions reduce the continuous load of particulate matter, thereby reducing BAOD. Meanwhile, the trend of the HAOD is related to air quality change associated with the intensity and frequency of severe aerosol events. Linear trends of seasonal BAOD and HAOD are analyzed here. In the trend analysis, BAOD or HAOD represent the average of the lowest or highest 5^{th} percentile of daily AODs per season in a year for each AERONET site. To avoid a bias in the long-term change analysis caused by different temporal sampling, the AERONET sites to be used are selected using the following criteria.

1. BAOD and HAOD are calculated when the number of observations exceeds 25 days per season in a year.
2. The seasonal dataset is composed of more than seven years of BAOD and HAOD values.

3. The dataset covers at least one year after 2016.

Using these criteria, we identified AERONET sites at which AOD measurements were made for >8 years between 1995 and 2019 (Figure 2). Of the 100 selected sites, 4 sites had <10 years of measurement, and 32 sites had >20 years of measurement.

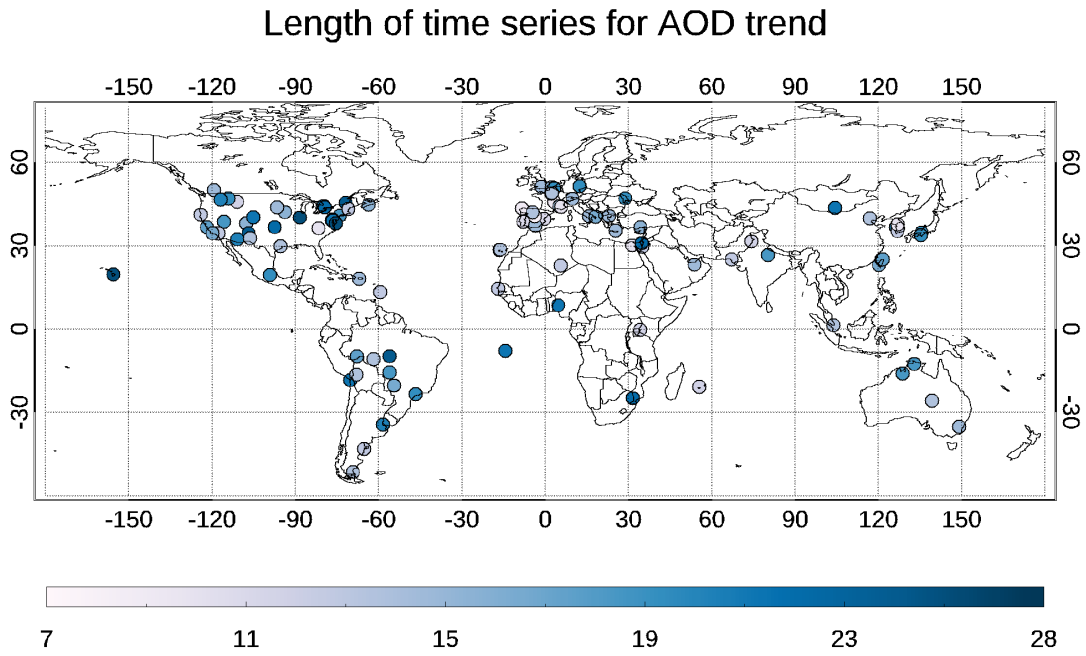

Figure 2. Locations of AERONET stations and length of data availability (years). The data period is denoted by the color scale.

The significance of the trend was determined based on the p-value test. When the p-value is less than 0.1, the trend is statistically significant at a 90% confidence level.

2.5. Study regions

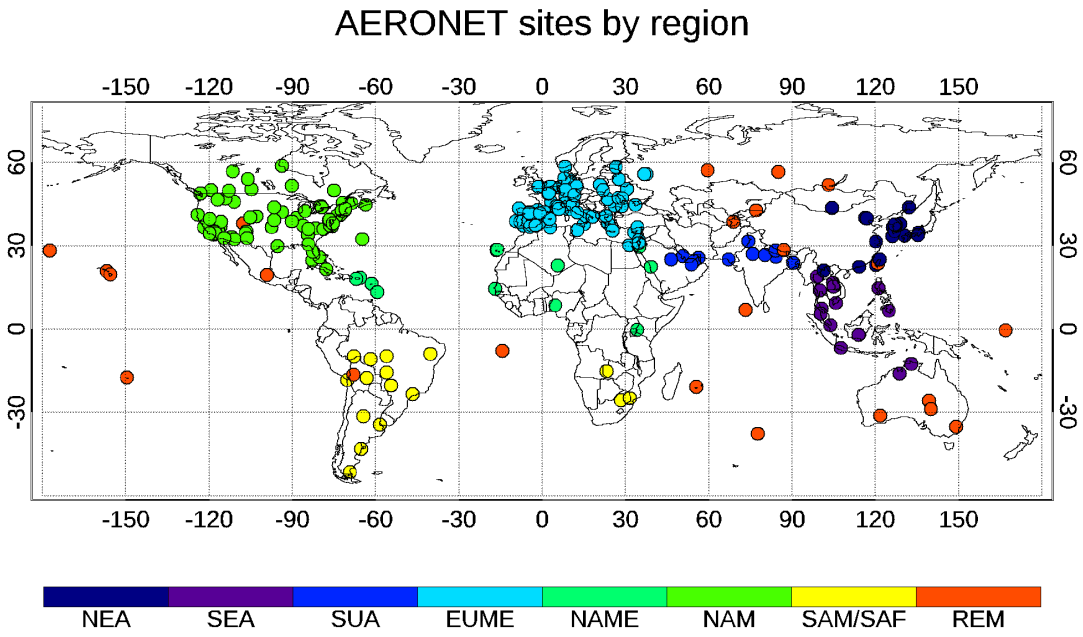

Figure 3. Assignment of AERONET sites to eight regions: Northeast Asia (NEA), Southeast Asia (SEA), South Asia (SUA), Europe/Mediterranean basin (EUME), North Africa/Middle East America (NAME), North America (NAM), South America/South Africa (SAM/SAF) and remote (REM) sites.

In this study, the seasonal characteristics of BAOD and its long-term trends were analyzed by categorizing AERONET sites into eight regions (Figure 3). AERONET sites were assigned using geolocation based on similar surface and aerosol conditions with reference to Sayer et al. (2018b). Major sources of aerosol emissions in each region are summarized in Table 1. Considering the low concentration of aerosols at high elevations, AERONET sites located higher than 2500 m were categorized as remote (REM) regions. Considering the dust transport across the Atlantic Ocean toward the Caribbean basin and Mediterranean basin (Goudie and Middleton, 2001), AERONET sites located near the Caribbean basin were combined with North Africa in this study.

247 Table 1. Summary of major aerosol sources in the eight regions defined in this study.

Region	Sources		Reference
Northeast Asia (NEA)	• Industry, automobiles and heating systems • Smoke from biomass burning • Dust transport • Smoke transported from boreal forest fires		Jung et al. (2016) Kim et al. (2010) Yoon et al. (2010)
Southeast Asia (SEA)	• Smoke from biomass burning		Huang et al. (2013) Lin et al. (2013)
South Asia (SUA)	• Smoke from agricultural burning • Anthropogenic pollution • Dust transport		David et al. (2018)
Europe/ Mediterranean basin (EUME)	• Fine particle formation • Dust transport		Kulmala et al. (2011) Nowak et al. (2010) Ma and Yu (2015) Zhao et al. (2018a)
North Africa/Middle East (NAME)	• Dust transport		Goudie and Middleton (2001)
North America (NAM)	West	• Wildfires over the northwest • Long-range dust and air pollutants • Locally emitted dust	Heald et al. (2006) Tong et al. (2012)
	East	• Fine particle formation	Nowak et al. (2010) Paulot et al. (2014) Xiao et al. (2013)
South America/ South Africa (SAM/SAF)	• Smoke from biomass burning		Castellanos et al. (2014) Mok et al. (2016) Roberts et al. (2009)
Remote (REM)	• Natural aerosol emissions (sea salt particles, dust, and volatile organic compounds (VOCs))		

248

249 **3. Results: Understanding spatial and seasonal variations in BAOD and HAOD**

250 *3.1. BAOD and HAOD from AERONET measurement*

251 *3.1.1. Global distributions*

252 Figure 4 presents global distributions of BAOD, HAOD and MAOD. High MAODs
253 are found in NEA, SEA, SUA, and Northwest Africa in Figure 4(a). The significant
254 regional variation in BAOD demonstrates its importance in both AOD retrieval and
255 assessing background air quality and the lower limit of radiative forcing (Figure 4(b)).
256 The BAODs show higher values in SUA and are moderately enhanced in NEA and
257 SEA. In eastern North America, Europe, and the SAM/SAF regions, BAODs remain at
258 a lower level in contrast to the enhanced MAOD. The maximum BAOD of 0.177 is

found at Lahore, which is the second largest city in Pakistan. The city is affected by air pollutant emissions from nearby factories in the iron, chemical, textile, and automobile industries, as well as thermal power plants. Automobile emissions, dust, and biomass burning are also reported to be major sources of air pollution in Lahore (Alam et al., 2012, Ali et al., 2014, Biswas et al., 2008). Aerosol properties are also affected by residential heating during the winter season and mineral dust during the pre-monsoon season (March to June; Ali et al., 2014). Similarly to the global BAOD distribution, the global HAOD distribution does not deviate widely from the MAOD distribution. However, the HAODs shown in Figure 4(c) are inconsistent with the MAOD in South Africa, South America, and boreal forest, where there is occasional intense biomass burning.

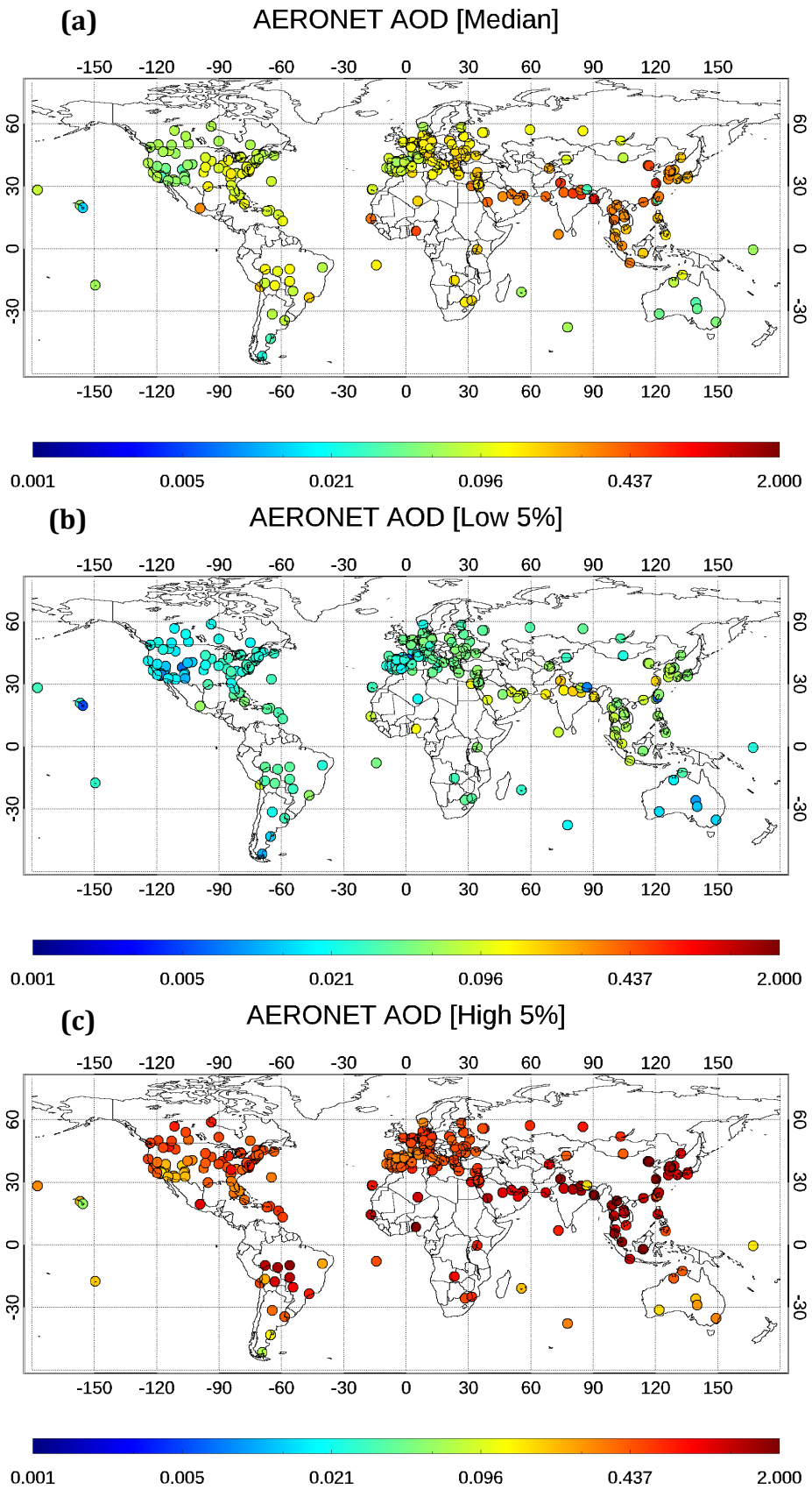

Figure 4. Distributions of (a) median AOD (MAOD) [550 nm], (b) background AOD (BAOD), and (c) high AOD (HAOD) obtained from AERONET direct measurement. BAOD and HAOD represent the average of AOD within the lowest 5th percentile and the highest 5th percentile, respectively.

278

279 *3.1.2. Variations in BAOD and HAOD by region*

280 *3.1.2.1. Seasonal characteristics*

281 While the MAOD in Figure 4(a) represents an average condition for the entire
282 data period, BAOD and HAOD are linked with specific meteorological events and/or
283 emission activities by season. To assess the seasonal variation in BAOD and HAOD,
284 the values in each region are compiled for four seasons (March–May, MAM; June–
285 August, JJA; September–November, SON; December–February, DJF) as shown in
286 Figure 5.

287

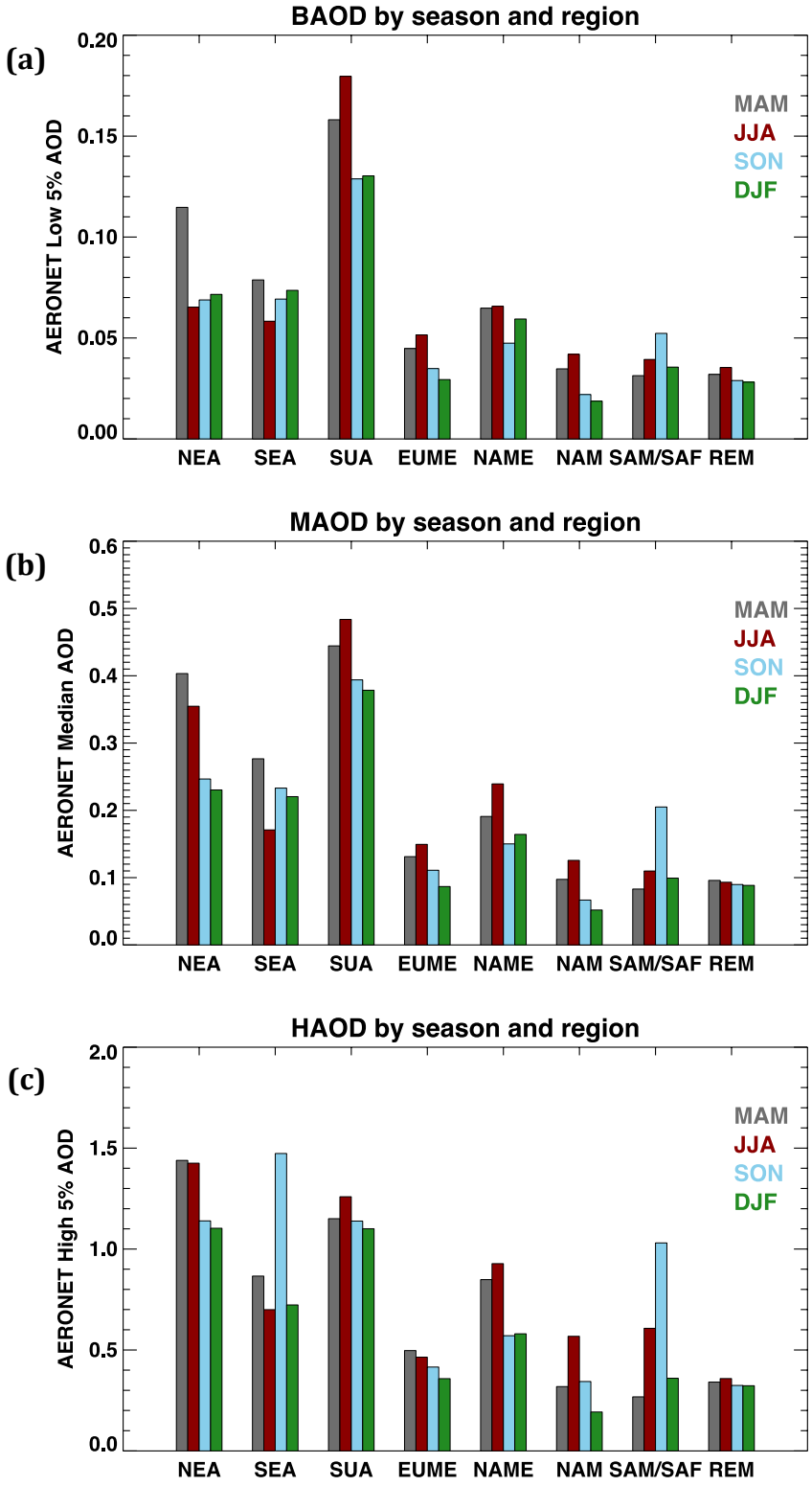

Figure 5. Seasonal variations in (a) BAOD (b) MAOD and (c) HAOD in eight regions. Bars show the average AODs for each season in the order MAM (March, April, and May), JJA (June, July, and August), SON (September, October, and November), and DJF (December, January, and February).

296 The seasonal changes in BAOD shown in Figure 5(a) are highly correlated with
297 MAOD (Figure 5(b)) in most regions. Notable differences between MAOD and BAOD
298 are found in NEA. In NEA, the highest value of BAOD is found during MAM, while
299 high levels of HAOD and MAOD continue during MAM and JJA (Figure 5(b,c)). Dust
300 transport from the Gobi and Taklamakan Deserts increases aerosol in the region during
301 local spring. Forest fires in Siberia can also cause severe aerosol loading during MAM
302 and JJA (Jung et al., 2016). Influenced by the stationary synoptic meteorological pattern
303 during JJA, secondary aerosol formation and hygroscopic growth of particles under
304 humid conditions lead to high MAOD (Kim et al., 2010, Liu et al., 2018, Yoon et al.,
305 2010). Under summer monsoon conditions, however, frequent precipitation washes out
306 accumulated air pollutants and contributes to a decrease in BAOD.
307 As shown in Figure 4(b) and Figure 5(a), BAODs in SUA are higher than in
308 other regions throughout the year because of continual aerosol emissions from both
309 anthropogenic and natural sources related to the high population density, a large
310 number of emission sources, and seasonal dust transport (Krotkov et al., 2016, Singh et
311 al., 2018). Dust blow from deserts in the Arabian Peninsula is largely responsible for
312 the highest BAOD values during JJA. The peak BAOD is significantly higher than the
313 values in other regions, whereas the HAODs stay at a similar level to the values in NEA
314 and SEA.
315 In the SAM/SAF and NAME regions, HAOD (Figure 5(c)) has more notable
316 seasonal change than BAOD (Figure 5(a)). In SAM/SAF, massive biomass burning
317 increases HAOD and MAOD during SON, but does not persist in other seasons.
318 Biomass burning is a recurring problem in Southeast Asia (SEA) as well (Huang et al.,
319 2013, Lin et al., 2013). However, BAODs in SAM/SAF are relatively lower than SEA,
320 consistent with the lack of continuous aerosol emissions from natural or anthropogenic

sources. In SEA, biomass burning results in synchronous increases in three AOD groups during MAM and SON, and continental air flow transports air pollutants and particles related to biomass burning from India or China under winter monsoon conditions between November and March (Sahu and Sheel, 2014). The diversity in aerosol sources leads to the higher BAOD in the region than in SAM/SAF.

3.2. BAOD and HAOD from VIIRS DB aerosol product

Satellite-based AOD products have the advantage of having higher spatial resolution than ground-based measurements. The VIIRS DB AODs cover both bright and dark surfaces, including the ocean, making them suitable for investigating the distributions of BAOD and HAOD for remote areas where anthropogenic contributions to the aerosol loads are limited.

Figure 6 shows a global distribution of the VIIRS DB AODs categorized as BAOD (Figure 6(a)), mean AOD (Figure 6(b)), and HAOD (Figure 6(c)). The white pixels indicate missing data, corresponding to insufficient measurements (<5% of the total period) due to frequent cloud cover or continuous snow cover over high-latitude or high-altitude regions. The distribution of missing data for BAOD and HAOD (Figure 6(a) and Figure 6(c)) is unlike that of the mean AODs in Figure 6(b). There are large amounts of missing data over the Amazon, Southeast Asia, south of the Sahara, the Tibetan Plateau, and the polar regions.

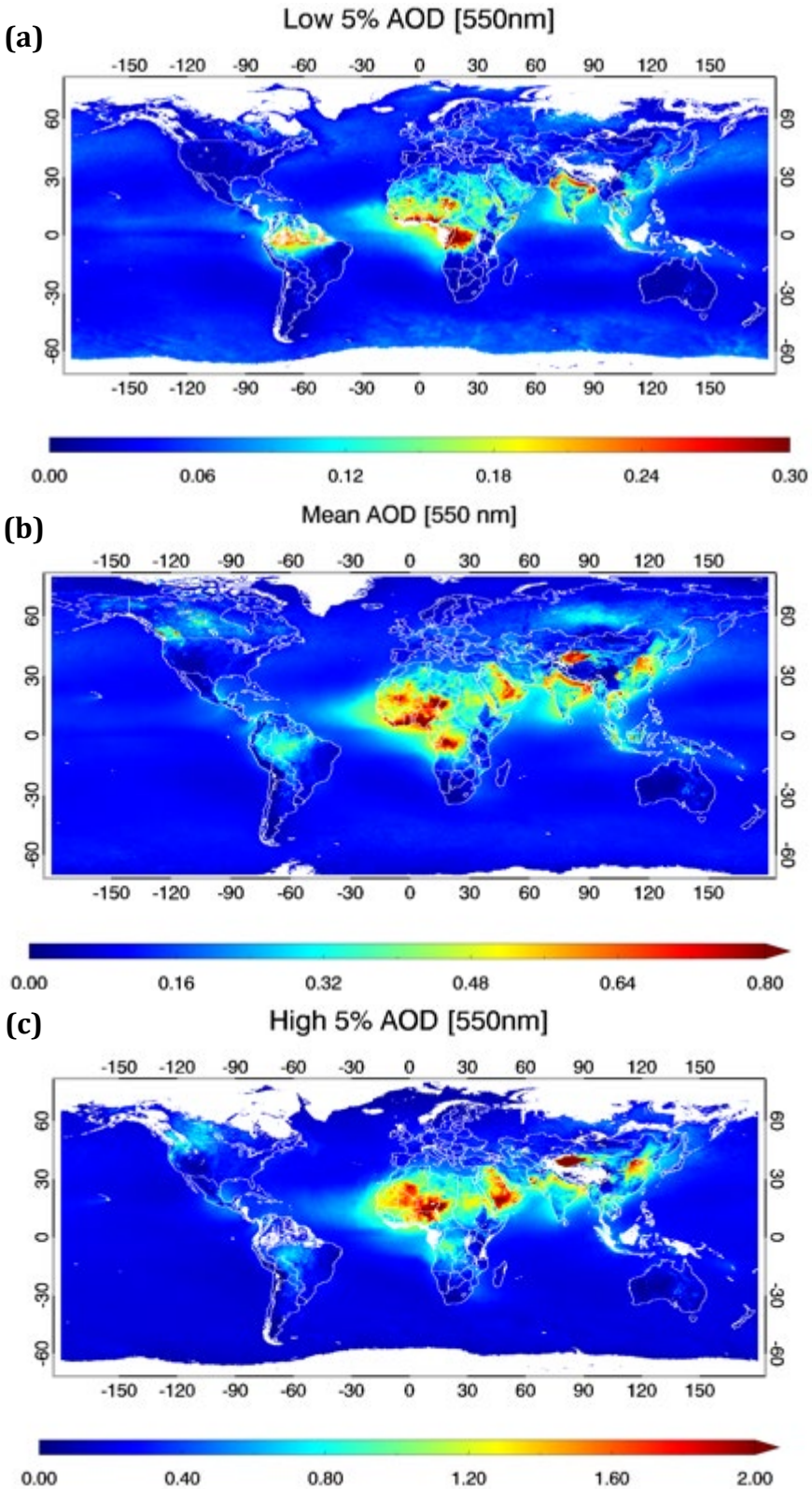

Figure 6. Distributions of (a) BAOD, (b) mean AOD, and (c) HAOD with 0.25° × 0.25° resolution obtained from VIIRS DB level 2 aerosol products from March 2012 to February 2019.

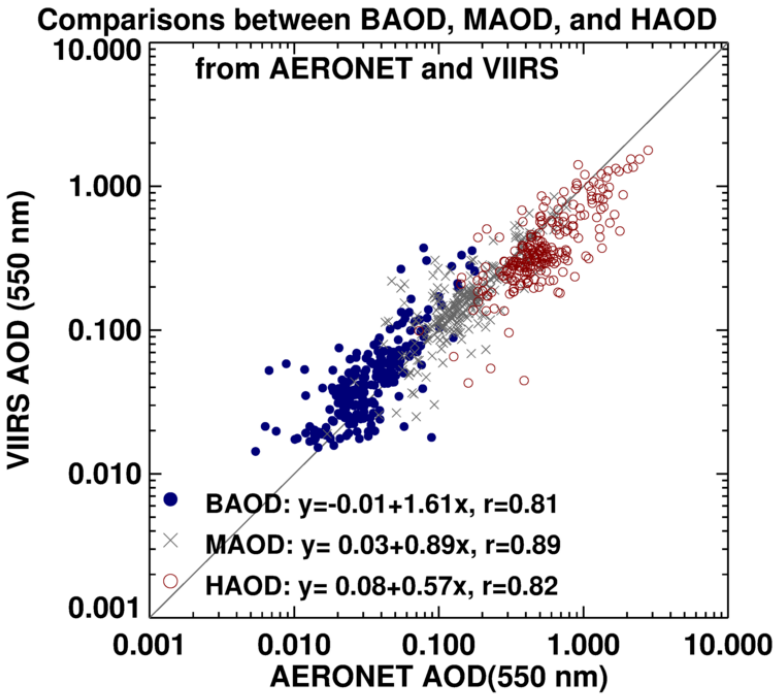

Figure 7. Comparisons between BAOD (blue filled circle), mean AOD (Gray x), and HAOD (red open circle) from AERONET and VIIRS in log scale. Solid gray line indicates 1:1 line.

Figure 7 presents comparisons between BAOD, mean AOD, and HAOD from VIIRS and AERONET. For the comparison, BAOD, mean AOD, and HAOD of the pixel closest to the location of the AERONET site were collocated with the AERONET values. The regression slope and correlation coefficient (r) indicate that the mean AOD comparison between AERONET and VIIRS products had the best agreement. VIIRS BAOD and HAOD tend to be overestimated and underestimated, respectively, compared with the AERONET values, but they correlate well with the AERONET values.

As the VIIRS DB AODs are highly validated against AERONET measurements (Figure 7), the distributions of AODs are well matched with the distributions of AERONET AODs shown in Figure 4. The three kinds of AOD distribution in Figure 6 show enhancement of AOD over known source regions including northern and central Africa, the Arabian Peninsula, India, and Southeast and Northeast Asia. BAODs are

differentiated from the mean and HAOD over northwestern North America, Russia, and Australia, which are influenced by episodic wildfires during regional dry seasons. Intense smoke injected into the upper tropospheric layer by wildfires significantly increases the AOD and is quickly spread by strong winds. Thus, episodic AOD enhancement increases the mean and HAOD values rather than BAOD. Accordingly, Figure 8 shows significant increases in HAOD during JJA owing to wildfires over the northwestern portion of North America and Russia (Figure 8(c)), compared with the weak seasonal variations in BAOD (Figure 9). In southern Africa, seasonal biomass burning activity induces a difference between BAOD and HAOD (Figure 6).

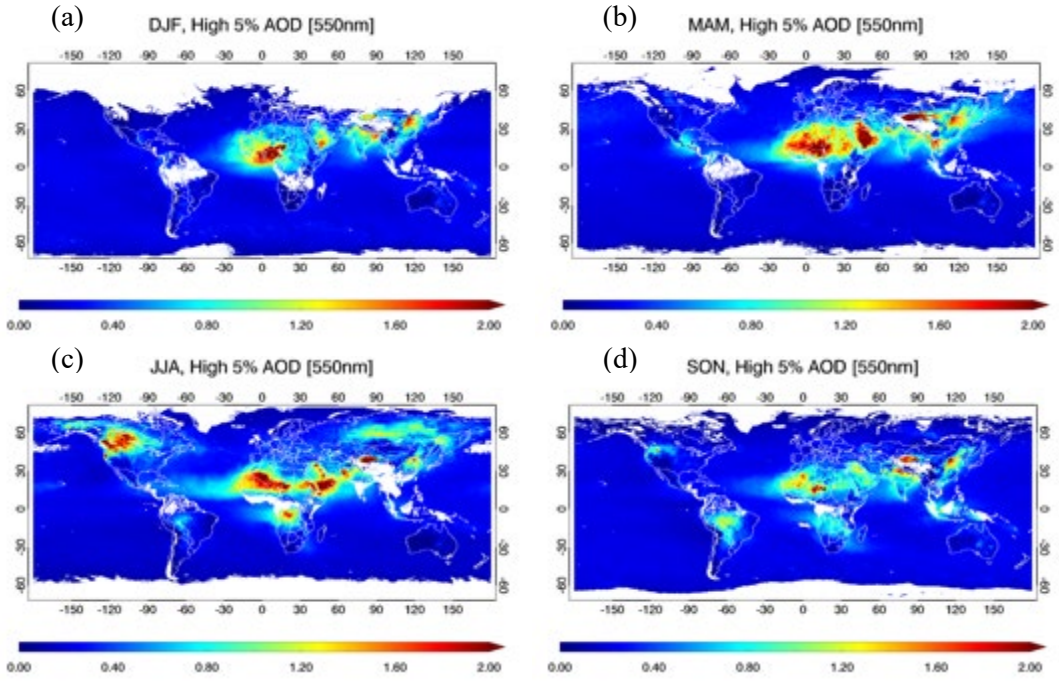

Figure 8. Maps of HAOD for the (a) DJF, (b) MAM, (c) JJA, and (d) SON seasons. The HAOD is calculated at each pixel that has >32 days AOD measurement for each season.

The aforementioned seasonal BAOD patterns are shown in Figure 9 with more detailed spatial variation. Regions of higher BAOD follow the seasonal pattern of distinctive seasonal biomass burning in Africa, characterized primarily by a peak in the Sahel during DJF and major fires during JJA and SON in Southern Africa (Figure 9).

High levels of BAOD caused by dust transport are notable during JJA throughout North Africa, the Arabian Peninsula, and the Arabian Sea. Over Northeast Asia, the winter monsoon circulation enhances the long-range transport of dust and air pollutants, and results in higher BAOD crossing the Northwest Pacific Ocean during DJF and MAM. BAOD increases mostly depend on natural emission patterns, but continuous emissions throughout the year increase BAOD in all seasons over the Indo-Gangetic Plain region (IGP, northeastern part of India).

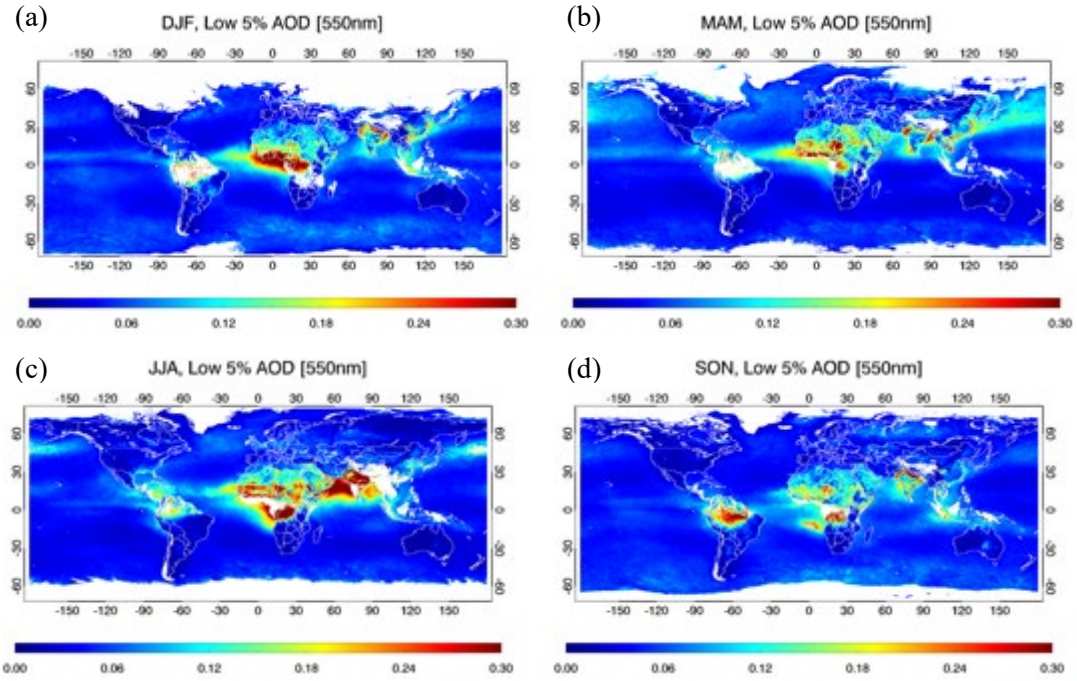

Figure 9. Same as Figure 8 but for BAOD.

The VIIRS BAOD map captures high levels of BAOD over both the known source regions described above, and also over ocean pixels neighboring inland source regions. Over the ocean, wind-driven sea-salt formation is a fundamental mechanism in the background aerosol loading. BAODs on open ocean areas show a homogeneous distribution in accordance with sea-salt formation. Near coastal areas, particle outflows from inland source regions are a major factor in enhancing background aerosol loadings.

Seasonal atmospheric changes in wind systems at different altitudes transport mineral dust from the Sahara Desert to Central America across the Atlantic Ocean, from the Arabian Peninsula to India across the Arabian Sea, and from the Gobi Desert and the Taklimakan Desert to the northwestern Pacific Ocean. Meanwhile, widespread smoke emissions from biomass burning activity over Africa, India, and Southeast Asia increase BAODs over the southern Atlantic Ocean, the Arabian Sea, and the western tropical Pacific Ocean, respectively.

3.3. Long-term changes in BAOD and HAOD

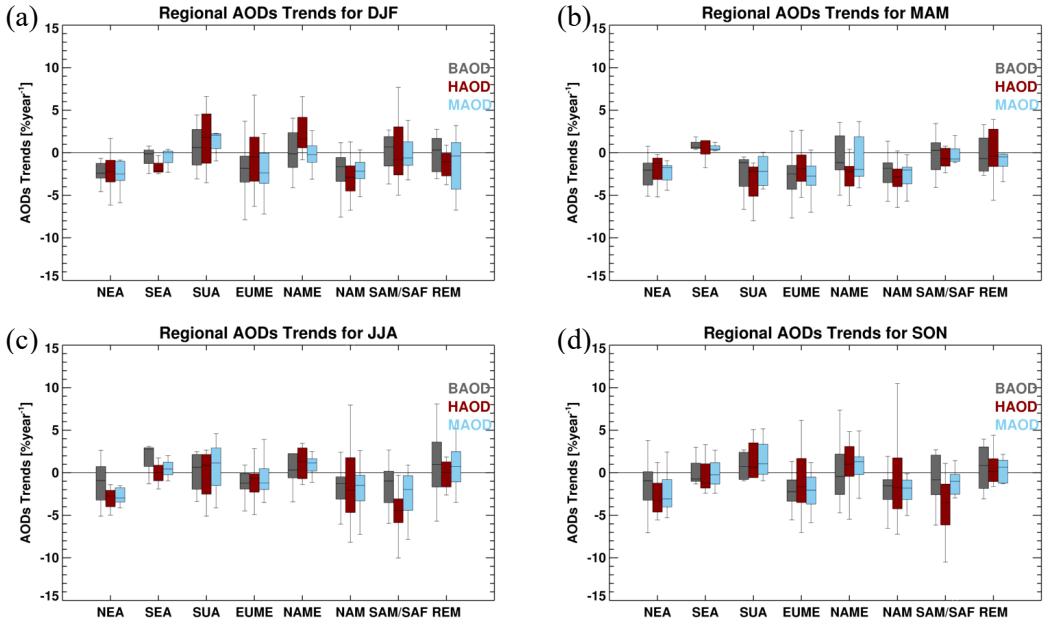

Figure 10. Box-and-whisker plots of BAOD trend [%year^{-1}] for each region in (a) DJF, (b) MAM, (c) JJA, and (d) SON.

Table 2. Mean trends and mean AODs for the eight regions. Values in parentheses are the standard deviation of AOD trends in each region.

Region	N	Season	BAOD		HAOD		MAOD	
			Mean Trend	Mean AOD	Mean Trend	Mean AOD	Mean Trend	Mean AOD
NEA	10	DJF	-2.18 (2.84)	0.08	-2.01 (2.40)	0.9	-2.21 (2.26)	0.23
		MAM	-2.27 (1.79)	0.12	-1.93 (1.73)	1.24	-2.19 (1.12)	0.40
		JJA	-1.12 (2.65)	0.07	-2.99 (1.13)	1.25	-2.75 (1.97)	0.36
		SON	-1.50 (3.03)	0.07	-2.79 (2.30)	0.96	-2.54 (2.34)	0.25
SEA	3	DJF	-0.59 (1.65)	0.07	-1.63 (1.15)	0.38	-0.63 (1.46)	0.15
		MAM	0.95 (0.80)	0.06	0.37 (1.85)	0.41	0.62 (0.54)	0.14
		JJA	1.53 (2.45)	0.05	-0.05 (1.83)	0.41	0.51 (1.49)	0.13
		SON	0.32 (2.34)	0.09	-0.10 (3.01)	0.74	-0.01 (2.53)	0.28
SUA	4	DJF	0.64 (3.09)	0.15	1.67 (4.19)	1.05	1.36 (1.57)	0.39
		MAM	-2.37 (2.88)	0.17	-3.39 (3.11)	0.99	-2.15 (2.05)	0.44
		JJA	0.10 (2.65)	0.27	-0.19 (3.44)	1.35	0.70 (3.60)	0.61
		SON	0.81 (1.87)	0.19	1.47 (2.69)	1.13	1.58 (2.59)	0.46
EUME	24	DJF	-1.88 (3.79)	0.04	-0.14 (4.13)	0.31	-1.84 (2.76)	0.09
		MAM	-2.79 (2.38)	0.05	-1.68 (2.19)	0.45	-2.75 (1.81)	0.14
		JJA	-1.32 (1.59)	0.06	-0.83 (1.92)	0.41	-0.45 (2.33)	0.15
		SON	-1.73 (3.41)	0.05	-1.12 (3.50)	0.36	-1.54 (2.99)	0.12
NAME	10	DJF	0.06 (2.63)	0.07	2.27 (2.45)	0.56	-0.19 (1.78)	0.18
		MAM	-0.63 (2.78)	0.08	-2.71 (2.01)	0.74	-0.94 (2.68)	0.20
		JJA	1.76 (3.98)	0.08	1.16 (1.89)	0.78	1.04 (1.94)	0.23
		SON	0.21 (3.67)	0.06	0.89 (2.98)	0.5	1.23 (2.33)	0.15
NAM	30	DJF	-2.03 (2.55)	0.02	-2.96 (4.53)	0.16	-2.65 (2.45)	0.05
		MAM	-2.33 (1.92)	0.04	-3.04 (1.97)	0.29	-2.69 (1.53)	0.10
		JJA	-1.68 (2.23)	0.05	-0.49 (5.48)	0.51	-1.75 (2.86)	0.13
		SON	-2.15 (2.42)	0.03	-0.33 (6.17)	0.32	-2.45 (3.24)	0.07
SAM/ SAF	11	DJF	0.17 (2.07)	0.04	0.26 (4.03)	0.29	0.02 (2.34)	0.10
		MAM	-0.20 (2.47)	0.04	-0.12 (2.99)	0.23	-0.30 (1.83)	0.09
		JJA	-1.90 (3.72)	0.05	-4.55 (2.67)	0.48	-3.01 (3.90)	0.12
		SON	-1.67 (4.76)	0.07	-3.96 (3.78)	0.83	-2.62 (4.60)	0.24
REM	8	DJF	-0.09 (2.23)	0.03	-3.10 (6.17)	0.24	-1.30 (3.43)	0.08
		MAM	-0.20 (2.27)	0.03	-0.02 (3.14)	0.24	-0.65 (1.76)	0.09
		JJA	1.03 (4.31)	0.03	-0.73 (2.91)	0.27	0.76 (2.73)	0.09
		SON	0.61 (2.68)	0.04	-0.44 (4.06)	0.29	0.34 (1.42)	0.10

To assess the impacts of anthropogenic activity and natural variation in aerosol emission on BAOD and HAOD, long-term changes in BAOD and HAOD must be investigated. Linear trends of AODs are regionally categorized and summarized in Figure 10 and Table 2. The seasonal BAOD and HAOD trends obtained from each AERONET site are displayed in Figure 11 and Figure 12. The averaged trends

summarized in Table 2 show that both BAOD and HAOD tend to decrease in most regions except SEA, SUA, and NAME.

NAME, a typical desert region, shows neutral or weak positive change in BAOD for less than 2% year^{-1}, except in MAM. The positive changes are also found in HAOD, especially over 2% year^{-1} in DJF. The increasing AODs can be influenced by decreasing precipitation over the Eastern Sahara (Pozzer et al., 2015, Yoon et al., 2016). Boiyo et al. (2018) also showed an increase in AOD values between 2002 and 2016 over East Africa, which is consistent with the reported increase in temperature and decrease in wind speed and precipitation. The increase in photochemical reactions and decrease in wet deposition associated with these meteorological conditions lead to the increase in AOD. However, both BAOD and HAOD showed negative trends in MAM, where dust transport is strong, and the seasonal change in HAOD is greater than the change in BAOD (Figure 10(b) and Table 2).

In SEA, BAOD and HAOD show a neutral trend that fluctuates around zero change throughout seasons. However, the limited number of AERONET sites (3 sites) in the SEA region makes identifying the regional trends difficult. A notable change in BAOD and HAOD are found in JJA (1.53% year^{-1} increase) and DJF (1.63% year^{-1} decrease), respectively, but the change is not more notable than other changes in different regions (Figure 11 and Figure 12).

SUA is going through rapid industrialization, and the massive economic growth influences the positive AOD trend (Hsu et al., 2012, Lee et al., 2018, Zhang and Reid, 2010). Accordingly, increasing trends are found in both BAOD and HAOD, except in MAM (Figure 10(b) and Table 2). David et al. (2018) showed that the AOD enhancement in the IGP region was associated with dust transport from the Arabian and Thar Deserts by westerly wind in both MAM and JJA/September. Meanwhile, Sahu

et al (2014) showed an enhancement of fire counts in India during MAM. Considering that the decreases in BAOD and HAOD are strong only in MAM, the changes are determined to be related to the changes in biomass burning.

Large decreases in both BAOD and HAOD are found in EUME and NEA, regardless of season. In those regions, strict environmental regulations have been applied to reduce anthropogenic pollutant emissions, and have resulted in a notable decrease in BAOD and HAOD. The European Environmental Agency reported a decrease in the main air pollutants between 1990 and 2016 as a result of restrictions on anthropogenic emissions (EEA, 2018), and many studies have reported decreasing AOD trends over Europe (De Meij et al., 2012, Hsu et al., 2012, Yoon et al., 2012). The negative trend in NEA is related to an improvement in life-related combustion systems for heating and power generation and the strengthening of pollutant emissions regulations (Zhao et al., 2018b). The tendencies of BAOD and HAOD agree with the MAOD trend, but BAODs are decreasing more rapidly than MAOD in both regions.

Negative trends in BAOD and HAOD are also found in NAM, but HAOD has a wide standard deviation (up to 6.17% $year^{-1}$) due to the opposite trends between the western and eastern part of NAM, in JJA and SON, in particular. While positive HAOD trends are dominant over the western part, negative trends are significant in the eastern part of NAM (Figure 12 (c), (d)).

In SAM/SAF, the decline in the deforestation rate and biomass burning has reduced aerosol emission (Pope et al., 2019). Burning causes massive aerosol emissions in a relatively short time period, which mainly enhances HAOD rather than BAOD (Figure 5). Accordingly, the rate of decrease of HAOD is greater than that of BAOD. Both BAOD and HAOD show neutral change in DJF and MAM but they showed a negative trend in JJA and SON, when biomass burning is increased. The decreasing

HAOD is -4.55% year^{-1} and -3.96% year^{-1} in JJA and SON, respectively, whereas the BAOD changes are less than 2% year^{-1} (Table 2).

Seasonal AODs obtained in REM stations showed a stagnant trend with a wide range (Figure 10 and Table 2). Inland sites over Australia revealed an increasing BAOD trend, while sites over the ocean showed stagnant trends (Figure 11 (b), (c)). Inland sites also have an opposite tendency for BAOD and HAOD in DJF, with HAOD decreasing, as opposed to the weak increase in BAOD. In the case of JJA, a large increase in BAOD appears unlike a weak change in HAOD. The results suggest that considering BAOD and HAOD in AOD trend analysis may be crucial for properly understanding trends.

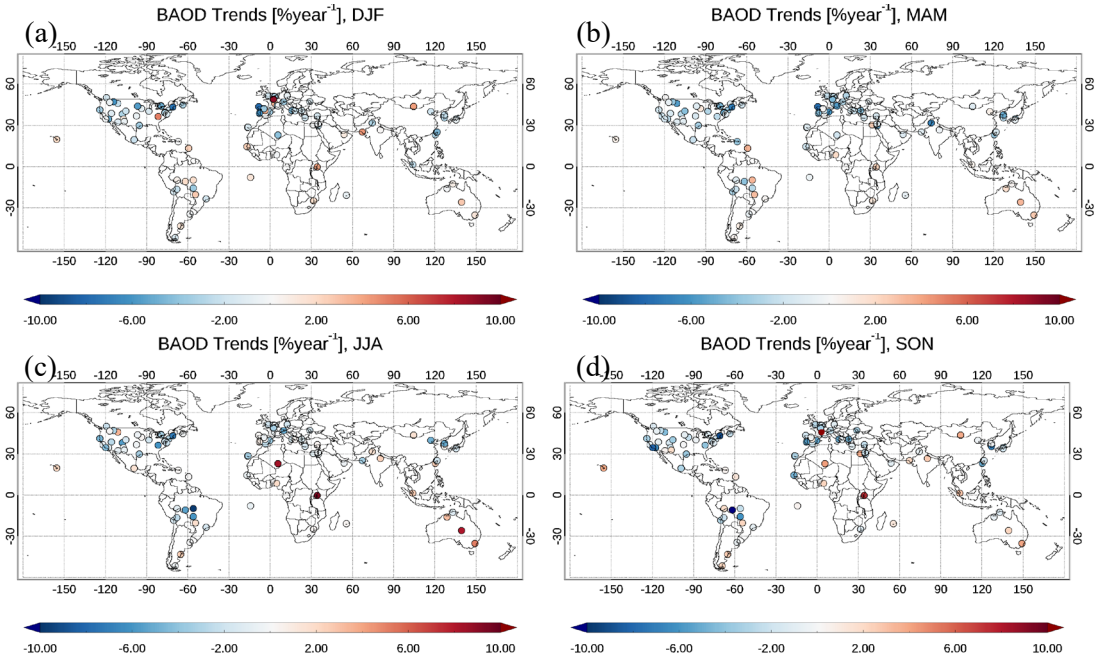

Figure 11. Linear trend [%year^{-1}] of BAOD in a season of (a) DJF, (b) MAM, (c) JJA, and (d) SON.

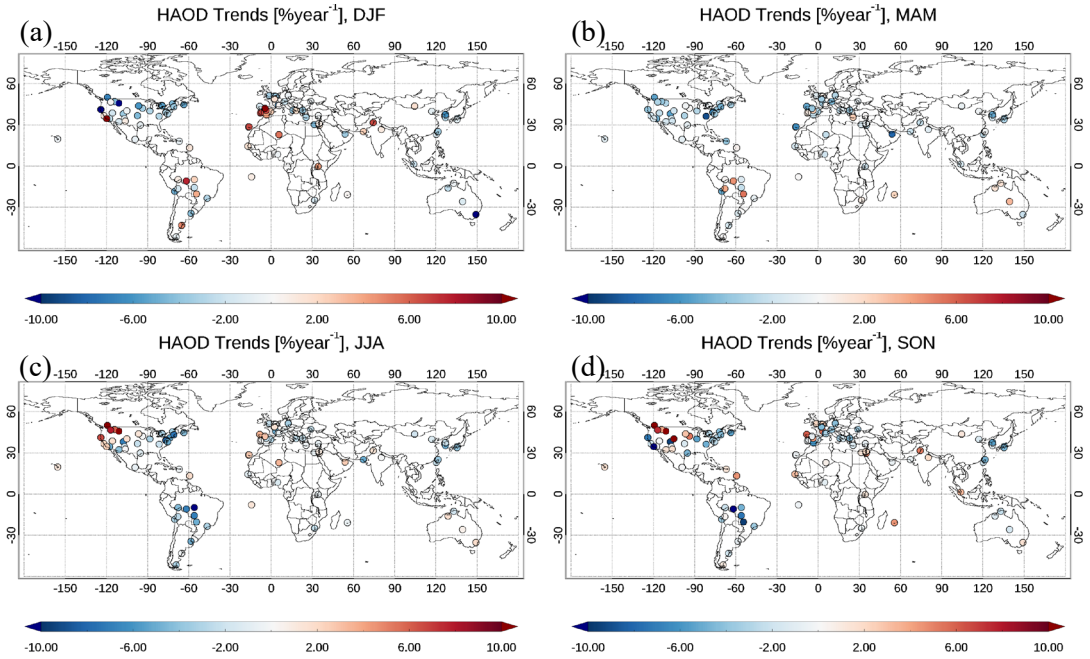

Figure 12. Same as Figure 11 but for HAOD.

Figure 13 shows an example of a locational p-value distribution obtained from the seasonal trend analysis in BAOD and HAOD. The figure shows that the BAOD and HAOD trends obtained from 36 and 31 of total 100 AERONET sites have p-value lower than 0.1. Higher than 0.1 p-value means the probability of observing a linear trend is higher than 10% when there is no linear trend. In Figure 14, percentage of the seasonal AODs trend having p-value lower than 0.1 among total site number is represented for each region. This figure shows that the trend analysis for each region contains at least 2 statistically significant trends, except for SUA and SEA, where there are insufficient numbers of AERONET sites.

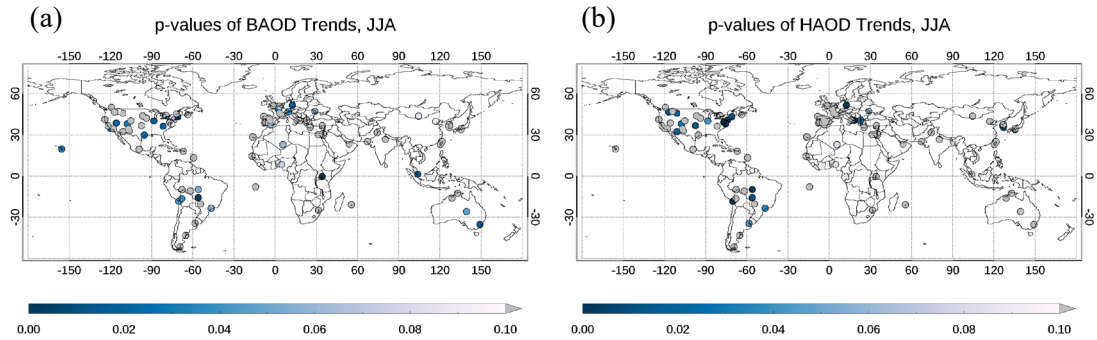

Figure 13. An example of p-value distribution obtained from the (a) BAOD and (b) HAOD in JJA. When the p-value is higher than 0.1, the value presented in gray.

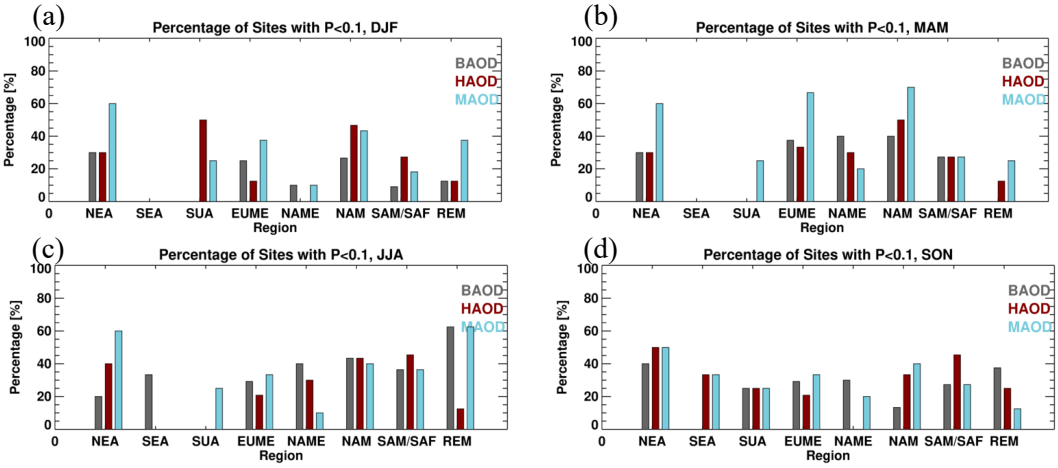

Figure 14. The percentage of AERONET sites that have statistically significant trends ($p<0.1$) at each region.

4. Summary and Discussion

In this study, global distributions and seasonal variations in BAOD and HAOD have been investigated using AERONET direct AOD measurements and VIIRS DB AOD products. BAOD was originally suggested to represent the minimal aerosol burden existing under background conditions without episodic emissions. Background aerosol loads result when continuous emissions accumulate more rapidly than the removal processes, and mainly depend on natural phenomena such as wind-blown sea salt or dust, and lightning-induced biomass burning. Air pollutants emitted from anthropogenic activity, such as agricultural burning and fossil fuel combustion, also increase persistent aerosol loading under background conditions. Accordingly, high

level BAOD values are found in regions with continuous anthropogenic activity as well as natural emission phenomena, such as NEA, SEA and SUA.

In previous studies, mean AOD has been widely adopted to investigate changes in AOD distribution. However, discrepancies between BAOD, HAOD, and MAOD were found, particularly in NEA. High MAOD induced by gas-to-particle formation and/or hygroscopic growth during JJA did not increase BAOD because of frequent precipitation under the summer monsoon conditions. Enhancement of BAOD is associated with the accumulation of particles, and it has a large sensitivity to both continuity of emissions and efficiency of removal. Therefore, BAOD can be more sensitive to weather than MAOD. During the rainy season (JJA) in NEA, low BAOD was found to result from washing out of aerosol particles and high MAOD and HAOD from gas-to-particle formation and hygroscopic growth. Variations of precipitation on longer than seasonal time scales (e.g. interannual) will also affect the AOD patterns but do not have a significant impact on our trend analysis based on mostly over 10 years of data.

In the comparison of regional variations in each AOD group (BAOD, HAOD, MAOD; Figure 5), BAOD and MAOD showed a remarkable elevation in SUA and NEA consistent with industrial and agricultural activity in those regions. High levels of BAODs were also found in the SEA and SAM/SAF regions, which were affected by biomass burning. Along with local biomass burning, long range transport of air pollutants and biomass burning products emitted from India or China also contribute to enhancing aerosol loading in SEA. Accordingly, BAOD was higher in SEA than in SAM/SAF.

In this study, VIIRS DB AOD products and AERONET station data were employed to analyze BAOD and HAOD distributions at a global scale. The global

555 distribution of VIIRS DB AOD showed seasonal enhancements of HAOD related to
556 intense smoke injection by wildfires over the northwestern part of North America,
557 Russia and Australia, and enhanced BAOD throughout the year in IGP in India and
558 NEA. The BAOD map captured the enhancement in BAOD over oceans adjoining
559 source regions. The gridded global BAOD distribution showed that massive aerosol
560 emissions and transport not only increased the values over source regions, but also
561 induced high levels of BAOD over oceans that adjoin Southern Africa and Asia. In
562 Africa, the VIIRS BAOD map revealed that values reached 0.3 around Central Africa
563 during DJF due to biomass burning.

564 The long-term variation in statistical AOD distribution has mainly been
565 analyzed based on its mean or median value. However, the three AOD groups showed
566 different variations in each region and season. The trend analyses indicate simultaneous
567 decreases of BAOD and HAOD in NEA and EUME. In EUME, the long-term negative
568 trends of BAOD, HAOD and MAOD varied between similar ranges since regulations
569 for pollutant emissions have successfully reduced the total aerosol burden. The strong
570 decrease in BAODs in NEA may be evidence for the success of social efforts to raise
571 awareness about air pollution problems. Dust transport is a major reason for heavy
572 aerosol loads in NEA in MAM, but the HAOD decrease, which is relatively lower than
573 in other seasons (Table 2), indicates that dust transport has not changed significantly.
574 Negative trends of BAOD and HAOD were also dominant in NAM, but HAODs in the
575 northwest of the region showed an increasing trend related to changes in wildfire
576 activity during JJA and SON. In SAM/SAF, the decrease in HAOD was significantly
577 greater than the decreases in BAOD, particularly during JJA and SON. The HAOD
578 trend indicated that the reduction in biomass burning associated with deforestation
579 significantly contributes to changes in aerosol loading. The linear trends of HAOD

(Figure 12) are correlated with the BAOD variations in general (Figure 11), but show notable differences in the northwest portion of North America and Australia that are affected by wildfires.

The significance of AOD trends were assessed using p-value in this study. Although most regions contain statistically significant trends in all seasons, the number of cases is limited in some regions and seasons. Because the trend analysis was conducted based on seasonal AODs obtained from 8 to 28 years of measurement (Figure 2), the time series for the linear trend calculation consists of fewer than 28 data points. The trend analysis that has insufficient data points could be biased due to an outlier. This weakness could be modified in a future study by the accumulation of measurements for a longer period. AERONET sites that are not evenly placed spatially increase uncertainty even in regional trend comparisons. Regionally averaged AOD trends listed in Table 2 may not have the same representability due to having different numbers of cases (i.e, AERONET site). For example, the trend in SEA was averaged from only 3 AERONET sites while the value in EUME was averaged from 24 sites. The regional imbalance in number of cases can be modified by adopting satellite-based AOD products that accumulate long-term measurements, such as MODIS. While employing satellite data increased the number of locations and datasets, the significance of detected trends will need to be further analyzed by adopting the false discovery rate (FDR; Wilks, 2016). The FDR procedure has been adapted to the climate context and will identify significance at the point by controlling the expected proportion of false-positives when multiple tests are conducted.

5. Conclusions

This study has investigated spatial and temporal variations in BAOD and HAOD in order to obtain a better understanding of aerosol loads. Compared to MAOD and HAOD, BAOD showed notable enhancement over the regions influenced by diverse emissions from natural phenomena and industrial activity. Over EUME, where decreasing anthropogenic pollutant emissions have been reported, there was a significant decrease in BAOD despite the low BAOD level. The results support the use of BAOD as an indicator to represent changes in the anthropogenic contribution to aerosol burden. Investigating the relation between BAOD and the anthropogenic contributions will be a further step in this study. We have investigated relative spatial and temporal variations in BAOD and HAOD rather than analyzing absolute values in a quantitative manner, given the uncertainties and limitations of AOD measurement. Low AOD values measured by remote sensing instruments are greatly affected by the calibration of the instruments. We obtained BAOD data using VIIRS measurement, but those values may be biased due to calibration issues and uncertainties in parameterization of surface reflectance. The quantitative values of BAOD and HAOD should be analyzed with other aerosol optical properties such as particle size distribution and radiative absorptivity. Results of the present study imply that further studies of BAOD analysis should adopt information about particle size and absorptivity under background conditions. In addition, merging ground-based and satellite-based BAODs will be necessary if BAOD is to be used as an input parameter in aerosol remote sensing algorithms.

Acknowledgements

We thank the PI(s) and Co-I(s) and their staff for establishing and maintaining the AERONET sites used in this investigation. Mijin's work was initiated at Chapman

University and completed during her NASA Postdoctoral Program (NPP). This paper is not funded or sponsored by NASA. This research was supported by the "Technology development for Practical Applications of Multi-Satellite data to maritime issues" funded by the Ministry of Ocean and Fisheries, Korea.

References

Alam, K., Trautmann, T., Blaschke, T., Majid, H., 2012. Aerosol optical and radiative properties during summer and winter seasons over Lahore and Karachi. Atmos Environ 50, 234-245.

Ali, M., Tariq, S., Mahmood, K., Daud, A., Batool, A., 2014. A study of aerosol properties over Lahore (Pakistan) by using AERONET data. Asia-Pacific Journal of Atmospheric Sciences 50, 153-162.

Biswas, K.F., Ghauri, B.M., Husain, L., 2008. Gaseous and aerosol pollutants during fog and clear episodes in South Asian urban atmosphere. Atmos Environ 42, 7775-7785.

Boiyo, R., Kumar, K.R., Zhao, T., 2018. Spatial variations and trends in AOD climatology over East Africa during 2002–2016: a comparative study using three satellite data sets. International Journal of Climatology 38, e1221-e1240.

Boucher, O., Randall, D., Artaxo, P., Bretherton, C., Feingold, G., Forster, P., Kerminen, V., Kondo, Y., Liao, H., Lohmann, U., Rasch, P., Satheesh, S., Sherwood, S., Stevens, B., Zhang, X., 2013. Clouds and Aerosols. In: Climate Change 2013: The Physical Science Basis. Contribution of Working Group I to the Fifth Assessment Report of the Intergovernmental Panel on Climate Change [Stocker, T.F., D. Qin, G.-K. Plattner, M. Tignor, S.K. Allen, J. Boschung, A. Nauels, Y. Xia, V. Bex and P.M. Midgley (eds.)]. Cambridge University Press, Cambridge, United Kingdom and New York, NY, USA.

Castellanos, P., Boersma, K., Van Der Werf, G., 2014. Satellite observations indicate substantial spatiotemporal variability in biomass burning NO x emission factors for South America. Atmospheric Chemistry and Physics 14, 3929-3943.

David, L.M., Ravishankara, A., Kodros, J.K., Venkataraman, C., Sadavarte, P., Pierce, J.R., Chaliyakunnel, S., Millet, D.B., 2018. Aerosol optical depth over India. Journal of Geophysical Research: Atmospheres 123, 3688-3703.

De Meij, A., Pozzer, A., Pringle, K., Tost, H., Lelieveld, J., 2012. EMAC model evaluation and analysis of atmospheric aerosol properties and distribution with a focus on the Mediterranean region. Atmospheric research 114, 38-69.

Eck, T.F., Holben, B., Reid, J., Dubovik, O., Smirnov, A., O'neill, N., Slutsker, I., Kinne, S., 1999. Wavelength dependence of the optical depth of biomass burning, urban, and desert dust aerosols. Journal of Geophysical Research: Atmospheres 104, 31333-31349.

EEA, 2018. European Union emission inventory report 1990 — 2016 under the UNECE Convention on Long-range Transboundary Air Pollution (LRTAP). European Environment Agency, Copenhagen, p. EEA technical report No 6/2018. Copenhagen.

672 Giles, D.M., Sinyuk, A., Sorokin, M.G., Schafer, J.S., Smirnov, A., Slutsker, I., Eck,
673 T.F., Holben, B.N., Lewis, J.R., Campbell, J.R., 2019. Advancements in the
674 Aerosol Robotic Network (AERONET) Version 3 database–automated near-real-
675 time quality control algorithm with improved cloud screening for Sun photometer
676 aerosol optical depth (AOD) measurements. Atmospheric Measurement
677 Techniques 12, 169-209.
678 Goudie, A., Middleton, N., 2001. Saharan dust storms: nature and consequences. Earth-
679 science reviews 56, 179-204.
680 Halthore, R.N., Caffrey, P.F., 2006. Measurement and modeling of background
681 aerosols in remote marine atmospheres: Implications for sea salt flux. Geophysical
682 research letters 33.
683 Halthore, R.N., Nemesure, S., Schwartz, S.E., Imre, D.G., Berk, A., Dutton, E.G.,
684 Bergin, M.H., 1998. Models overestimate diffuse clear-sky surface irradiance: A
685 case for excess atmospheric absorption. Geophysical research letters 25, 3591-3594.
686 Heald, C.L., Jacob, D.J., Park, R.J., Alexander, B., Fairlie, T.D., Yantosca, R.M., Chu,
687 D.A., 2006. Transpacific transport of Asian anthropogenic aerosols and its impact
688 on surface air quality in the United States. Journal of Geophysical Research:
689 Atmospheres 111.
690 Holben, B., Tanre, D., Smirnov, A., Eck, T., Slutsker, I., Abuhassan, N., Newcomb, W.,
691 Schafer, J., Chatenet, B., Lavenu, F., 2001. An emerging ground-based aerosol
692 climatology: Aerosol optical depth from AERONET. Journal of Geophysical
693 Research: Atmospheres 106, 12067-12097.
694 Holben, B.N., Eck, T.F., Slutsker, I., Tanre, D., Buis, J., Setzer, A., Vermote, E.,
695 Reagan, J.A., Kaufman, Y., Nakajima, T., 1998. AERONET—A federated
696 instrument network and data archive for aerosol characterization. Remote sensing
697 of environment 66, 1-16.
698 Hsu, N., Gautam, R., Sayer, A., Bettenhausen, C., Li, C., Jeong, M., Tsay, S., Holben,
699 B., 2012. Global and regional trends of aerosol optical depth over land and ocean
700 using SeaWiFS measurements from 1997 to 2010.
701 Hsu, N., Lee, J., Sayer, A., Kim, W., Bettenhausen, C., Tsay, S.C., 2019. VIIRS Deep
702 Blue Aerosol Products over Land: Extending the EOS Long-Term Aerosol Data
703 Records. Journal of Geophysical Research: Atmospheres.
704 Huang, K., Fu, J.S., Hsu, N.C., Gao, Y., Dong, X., Tsay, S.-C., Lam, Y.F., 2013. Impact
705 assessment of biomass burning on air quality in Southeast and East Asia during
706 BASE-ASIA. Atmos Environ 78, 291-302.
707 Jung, J., Lyu, Y., Lee, M., Hwang, T., Lee, S., Oh, S., 2016. Impact of Siberian forest
708 fires on the atmosphere over the Korean Peninsula during summer 2014.
709 Atmospheric Chemistry and Physics 16, 6757-6770.
710 Kaufman, Y.J., Smirnov, A., Holben, B.N., Dubovik, O., 2001. Baseline maritime
711 aerosol: methodology to derive the optical thickness and scattering properties.
712 Geophysical Research Letters 28, 3251-3254.
713 Kaufman, Y.J., Tanré, D., Boucher, O., 2002. A satellite view of aerosols in the climate
714 system. Nature 419, 215-223.
715 Kim, M., Kim, J., Jeong, U., Kim, W., Hong, H., Holben, B., Eck, T.F., Lim, J.H., Song,
716 C.K., Lee, S., 2016. Aerosol optical properties derived from the DRAGON-NE Asia
717 campaign, and implications for a single-channel algorithm to retrieve aerosol
718 optical depth in spring from Meteorological Imager (MI) on-board the
719 Communication, Ocean, and Meteorological Satellite (COMS). Atmospheric
720 Chemistry and Physics 16, 1789-1808.

721 Kim, M., Kim, J., Wong, M.S., Yoon, J., Lee, J., Wu, D., Chan, P., Nichol, J.E., Chung,
722 C.-Y., Ou, M.-L., 2014. Improvement of aerosol optical depth retrieval over Hong
723 Kong from a geostationary meteorological satellite using critical reflectance with
724 background optical depth correction. Remote sensing of environment 142, 176-187.
725 Kim, S.-W., Choi, I.-J., Yoon, S.-C., 2010. A multi-year analysis of clear-sky aerosol
726 optical properties and direct radiative forcing at Gosan, Korea (2001–2008).
727 Atmospheric Research 95, 279-287.
728 Knapp, K.R., Frouin, R., Kondragunta, S., Prados, A., 2005. Toward aerosol optical
729 depth retrievals over land from GOES visible radiances: determining surface
730 reflectance. International Journal of Remote Sensing 26, 4097-4116.
731 Krotkov, N.A., McLinden, C.A., Li, C., Lamsal, L.N., Celarier, E.A., Marchenko, S.V.,
732 Swartz, W.H., Bucsela, E.J., Joiner, J., Duncan, B.N., 2016. Aura OMI observations
733 of regional SO 2 and NO 2 pollution changes from 2005 to 2015. Atmospheric
734 Chemistry and Physics 16, 4605-4629.
735 Kulmala, M., Asmi, A., Lappalainen, H., Baltensperger, U., Brenguier, J.-L., Facchini,
736 M., Hansson, H.-C., Hov, Ø., O'Dowd, C., Pöschl, U., 2011. General overview:
737 European Integrated project on Aerosol Cloud Climate and Air Quality interactions
738 (EUCAARI)–integrating aerosol research from nano to global scales. Atmospheric
739 Chemistry and Physics 11, 13061-13143.
740 Lee, H.-H., Iraqui, O., Gu, Y., Yim, S.H.-L., Chulakadabba, A., Tonks, A.Y.-M., Yang,
741 Z., Wang, C., 2018. Impacts of air pollutants from fire and non-fire emissions on
742 the regional air quality in Southeast Asia. Atmospheric Chemistry and Physics 18,
743 6141-6156.
744 Lin, N.-H., Tsay, S.-C., Maring, H.B., Yen, M.-C., Sheu, G.-R., Wang, S.-H., Chi, K.H.,
745 Chuang, M.-T., Ou-Yang, C.-F., Fu, J.S., 2013. An overview of regional
746 experiments on biomass burning aerosols and related pollutants in Southeast Asia:
747 From BASE-ASIA and the Dongsha Experiment to 7-SEAS. Atmos Environ 78, 1-
748 19.
749 Liu, B., Ma, Y., Gong, W., Zhang, M., Wang, W., Shi, Y., 2018. Comparison of AOD
750 from CALIPSO, MODIS, and sun photometer under different conditions over
751 central China. Scientific reports 8, 1-10.
752 Ma, X., Yu, F., 2015. Seasonal and spatial variations of global aerosol optical depth:
753 multi-year modelling with GEOS-Chem-APM and comparisons with multiple-
754 platform observations. Tellus B: Chemical and Physical Meteorology 67, 25115.
755 Mok, J., Krotkov, N.A., Arola, A., Torres, O., Jethva, H., Andrade, M., Labow, G., Eck,
756 T.F., Li, Z., Dickerson, R.R., 2016. Impacts of brown carbon from biomass burning
757 on surface UV and ozone photochemistry in the Amazon Basin. Scientific reports
758 6, 36940.
759 Nowak, J., Neuman, J., Bahreini, R., Brock, C., Middlebrook, A., Wollny, A.,
760 Holloway, J., Peischl, J., Ryerson, T., Fehsenfeld, F., 2010. Airborne observations
761 of ammonia and ammonium nitrate formation over Houston, Texas. Journal of
762 Geophysical Research: Atmospheres 115.
763 Paulot, F., Jacob, D.J., Pinder, R., Bash, J., Travis, K., Henze, D., 2014. Ammonia
764 emissions in the United States, European Union, and China derived by high-
765 resolution inversion of ammonium wet deposition data: Interpretation with a new
766 agricultural emissions inventory (MASAGE_NH3). Journal of Geophysical
767 Research: Atmospheres 119, 4343-4364.
768 Pope, R.J., Arnold, S.R., Chipperfield, M.P., Reddington, C.L., Butt, E.W., Keslake,
769 T.D., Feng, W., Latter, B.G., Kerridge, B.J., Siddans, R., 2019. Substantial

increases in Eastern Amazon and Cerrado biomass burning-sourced tropospheric ozone. Geophysical Research Letters.
Pozzer, A., De Meij, A., Yoon, J., Tost, H., Georgoulias, A., Astitha, M., 2015. AOD trends during 2001–2010 from observations and model simulations. Atmospheric Chemistry and Physics 15, 5521-5535.
Roberts, G., Wooster, M., Lagoudakis, E., 2009. Annual and diurnal african biomass burning temporal dynamics. Biogeosciences 6, 849-866.
Sahu, L., Sheel, V., 2014. Spatio-temporal variation of biomass burning sources over South and Southeast Asia. Journal of Atmospheric Chemistry 71, 1-19.
Sayer, A., Hsu, N., Lee, J., Bettenhausen, C., Kim, W., Smirnov, A., 2018a. Satellite Ocean Aerosol Retrieval (SOAR) Algorithm Extension to S-NPP VIIRS as Part of the "Deep Blue" Aerosol Project. Journal of Geophysical Research: Atmospheres 123, 380-400.
Sayer, A.M., Hsu, N.C., Lee, J., Kim, W.V., Dubovik, O., Dutcher, S.T., Huang, D., Litvinov, P., Lyapustin, A., Tackett, J.L., 2018b. Validation of SOAR VIIRS Over-Water Aerosol Retrievals and Context Within the Global Satellite Aerosol Data Record. Journal of Geophysical Research: Atmospheres 123, 13,496-413,526.
Sayer, A. M., Hsu, N. C., Lee, J., Kim, W. V., Dutcher, S. T., 2019. Validation, stability, and consistency of MODIS Collection 6.1 and VIIRS Version 1 Deep Blue aerosol data over land. Journal of Geophysical Research: Atmospheres, 124(8), 4658-4688.
Singh, R., Kumar, S., Singh, A., 2018. Elevated Black Carbon Concentrations and Atmospheric Pollution around Singrauli Coal-Fired Thermal Power Plants (India) Using Ground and Satellite Data. International journal of environmental research and public health 15, 2472.
Tong, D.Q., Dan, M., Wang, T., Lee, P., 2012. Long-term dust climatology in the western United States reconstructed from routine aerosol ground monitoring. Atmospheric Chemistry and Physics 12, 5189-5205.
Wilks, D. S., 2016. The stippling shows statistically significant grid points: How research results are routinely overstated and overinterpreted, and what to do about it. Bull. Amer. Meteor. Soc., 97, 2263–2273, https://doi.org/10.1175/BAMS-D-15-00267.1.
Xiao, Z., Jiang, H., Song, X., Zhang, X., 2013. Monitoring of atmospheric nitrogen dioxide using Ozone Monitoring Instrument remote sensing data. Journal of Applied Remote Sensing 7, 073534.
Yoon, J., Pozzer, A., Chang, D.Y., Lelieveld, J., Kim, J., Kim, M., Lee, Y., Koo, J.-H., Lee, J., Moon, K., 2016. Trend estimates of AERONET-observed and model-simulated AOTs between 1993 and 2013. Atmos Environ 125, 33-47.
Yoon, J., von Hoyningen-Huene, W., Kokhanovsky, A.A., Vountas, M., Burrows, J.P., 2012. Trend analysis of aerosol optical thickness and Ångström exponent derived from the global AERONET spectral observations. Atmos. Meas. Tech. 5, 1271-1299.
Yoon, S.-C., Kim, S.-W., Choi, S.-J., Choi, I.-J., 2010. Regional-scale relationships between aerosol and summer monsoon circulation, and precipitation over northeast Asia. Asia-Pacific Journal of Atmospheric Sciences 46, 279-286.
Zhang, H., Kondragunta, S., Laszlo, I., Liu, H., Remer, L.A., Huang, J., Superczynski, S., Ciren, P., 2016. An enhanced VIIRS aerosol optical thickness (AOT) retrieval algorithm over land using a global surface reflectance ratio database. Journal of Geophysical Research: Atmospheres 121, 10,717-710,738.

Zhang, H., Lyapustin, A., Wang, Y., Kondragunta, S., Laszlo, I., Ciren, P., Hoff, R., 2011. A multi-angle aerosol optical depth retrieval algorithm for geostationary satellite data over the United States. Atmospheric Chemistry & Physics 11.
Zhang, J., Reid, J., 2010. A decadal regional and global trend analysis of the aerosol optical depth using a data-assimilation grade over-water MODIS and Level 2 MISR aerosol products. Atmospheric Chemistry and Physics 10, 10949-10963.
Zhao, B., Jiang, J.H., Diner, D.J., Su, H., Gu, Y., Liou, K.-N., Jiang, Z., Huang, L., Takano, Y., Fan, X., 2018a. Intra-annual variations of regional aerosol optical depth, vertical distribution, and particle types from multiple satellite and ground-based observational datasets. Atmospheric chemistry and physics 18, 11247-11260.
Zhao, B., Zheng, H., Wang, S., Smith, K.R., Lu, X., Aunan, K., Gu, Y., Wang, Y., Ding, D., Xing, J., 2018b. Change in household fuels dominates the decrease in PM2. 5 exposure and premature mortality in China in 2005–2015. Proceedings of the National Academy of Sciences 115, 12401-12406.